Image Change Detection Based on Fuzzy Clustering and Neural Networks

Chenwei Wang, Xiating Li*
School of Information Engineering, Jiangxi V&T College of Communications, Nanchang, 330013, China

***Abstract*—In the change detection of synthetic aperture radar images, the image quality and change detection accuracy are difficult to meet the application requirements due to the influence of speckle noise. Therefore, the study improved the fuzzy C-means algorithm by introducing fuzzy membership degree and Gabor texture features. Features were weighted through channel attention, resulting in an image change detection model, namely, the fuzzy local information C-means for Gabor textures and multi-scale channel attention wavelet convolutional neural network. The segmentation accuracy of the model was 0.995, which improved by 0.119 compared to the traditional fuzzy C-means algorithm. When adding multiplicative noise with different variances, the noise variance reached 0.30, and the accuracy of the algorithm still reached 0.982. In practical application analysis, the detection and segmentation accuracy of river images was 0.983 with a partition coefficient of 0.935, and the segmentation accuracy of farmland images was 0.960 with a partition coefficient of 0.902. Therefore, the algorithm has good stability and anti-noise performance. The algorithm can be widely applied in various fields of synthetic aperture radar image change detection, such as disaster assessment, urban development monitoring, and environmental change monitoring. This paper provides more accurate analysis results, which help with policy formulation and effective resource management.**

Keywords*—Fuzzy C-means algorithm; fuzzy membership degree; Gabor texture; channel attention; neural networks; synthetic aperture radar images

I. INTRODUCTION

The current Synthetic Aperture Radar (SAR) imaging technology plays an important role in multiple fields, such as environmental monitoring, geological exploration, etc. [1]. However, SAR images are inevitably affected by speckle noise in imaging. The speckle noise can seriously reduce image quality and have adverse effects on subsequent image processing and applications. Especially when conducting change detection, the presence of noise can significantly reduce the accuracy and reliability of the detection [2]. During the development of computer vision and machine learning technology, SAR Image Change Detection (ICD) has achieved certain results [3-4]. However, deep learning methods still have certain shortcomings in dealing with speckle noise and preserving image details. The main challenges faced by SAR ICD are how to effectively suppress speckle noise, how to preserve detailed information in the image, and how to improve the accuracy and robustness of change detection. To solve the suppressing speckle noise and preserving image details, a new ICD model was proposed, namely Fuzzy Local Information C-means for Gabor Textures and Multi-scale Channel Attention-Wavelet Convolutional Neural Network (GT-FLICM-MSCA-WCNN). The significance of this research is that the SAR image processing effect can be effectively improved and the development of image technology can be promoted. The research contribution is to construct a Multi-Scale Channel Attention-Wavelet Convolutional Neural Network (MSCA-WCNN) by combining fuzzy membership degree and Gabor texture feature improved Fuzzy C-means (FCM) algorithm, which enhances the speckle noise suppression ability and improves ICD effect. The innovation of the method lies in suppressing speckle noise by combining Gabor texture features and fuzzy local information and increasing the weight of important image features through Channel Attention (CA). The research content mainly includes four parts. Firstly, the research achievements of domestic and foreign scholars on ICD are summarized. Secondly, the improved FCM algorithm and MSCA-WCNN are constructed separately. Then, performance analysis is conducted on the constructed model to verify the ability to suppress noise and Segmentation Accuracy (SA). Finally, the research results are summarized, and the shortcomings and future research directions are pointed out.

II. RELATED WORKS

A. Research achievements related to ICD

In ICD, many scholars have proposed many methods and achieved certain results. Ghosh C et al. proposed a spatial perceptual FCM-based model for change detection in SAR images, which utilized CNN for sample training and testing. Through experimental analysis, the model had good false detection performance and effectively sought differences in images [5]. Su et al. proposed an unsupervised method based on a fecal autoencoder network, which utilized non-local feature learning to detect area changes in ASR images. The recognition accuracy of the method reached 99.72%, proving the good robustness the method [6]. Li et al. proposed an image detection model based on iterative guided filtering for SAR change detection, which also introduced logarithmic mean ratio to enhance the model's trend of change. In dataset testing, the method improved the accuracy of change detection [7]. Wang et al. proposed a graph-based knowledge supplementation network that extracted feature value target datasets and sought the correlation between features and datasets. In comparative experiments, the method demonstrated superior ICD performance compared to current advanced methods [8].

FCM and CNN have many applications in ICD. Ghosh C et al. proposed an ICD model based on modified Gaussian contrast number and fuzzy local information C-means

clustering. The model completed the change of image pixels through fuzzy local information C-means clustering and classified them through CNN. The results showed high stability and running efficiency [9]. Peng et al. proposed an ICD model of SAR based on visual saliency and multi-level fuzzy clustering, which identified potential change regions through FCM. In the comparative experiment, the detection accuracy of the model was 99.07%, and the Kappa coefficient was 79.87%, demonstrating good performance [10]. Yi et al. proposed an ICD model based on Gabor wavelets and convolutional wavelet neural networks. The model combined Gabor wavelets with FCM to solve the low pre-classification accuracy and showed good detection performance on real datasets [11]. Zhang et al. proposed a fast non-local clustering algorithm to classify ASR images, effectively preserving the details of image change regions and suppressing the influence of noise, thereby improving the ICD quality of ASR [12].

B. Comparative Analysis

Among the above methods, although the method proposed by Ghosh C et al. and Peng Y et al. could solve the false detection and potential change region identification in ICD to a certain extent, the suppression effect of speckle noise in SAR images was limited. The methods proposed by Su H et al. and Wang J et al. relied on models such as deep learning and autoencoder networks. These methods performed well in non-local feature learning and feature extraction. However, these methods may lack robustness and stability in the face of different noise levels. The methods of Li W T et al. and Zhang W et al. introduced iterative guided filtering and non-local clustering algorithms in the detection and classification of image change trends, which performed well in the accuracy of change detection. However, these methods may still be inadequate in handling detailed retention of SAR images. Although Ghosh C et al.'s approach combined fuzzy local information, the performance could still be compromised in high-noise environments. Therefore, a new method GT-FLICM-MSCA-WCNN is proposed. Compared with the current research methods, this paper introduces fuzzy membership degree and Gabor texture features to improve the FCM algorithm, which makes the improved algorithm better deal with speckle noise. Gabor texture features can effectively capture the texture information in the image, improve the noise suppression effect, and retain the image details. Combined with wavelet transform to process multi-scale information, the noise is effectively suppressed. The multi-level details of the image are preserved, and the accuracy and reliability of ICD are improved.

III. Image Change Detection Based on Improved FCM and WCNN

This study introduces the application of fuzzy clustering and neural networks in SAR image processing to solve the image quality degradation caused by speckle noise in ICD of SAR. Firstly, the study improves traditional FCM by introducing a fuzzy membership degree. Secondly, a pre-classification model for SAR images is constructed by combining Gabor texture features and fuzzy local information. Finally, MSCA is introduced to improve Wavelet Convolutional Neural Network (WCNN).

A. Construction of SAR Imaging and Fuzzy C-Means Algorithm

The study detects and analyzes the changes in SAR images. The image formation is closely related to the direction, azimuth, and distance of radar motion. Usually, SAR systems are combined with relevant carrier platforms to move at a constant speed and emit electromagnetic waves towards the target detection area for scanning. The interval between each emission of electromagnetic waves is the same. Then, the echo signals are collected to obtain high-resolution images [13]. Fig. 1 shows the specific SAR imaging.

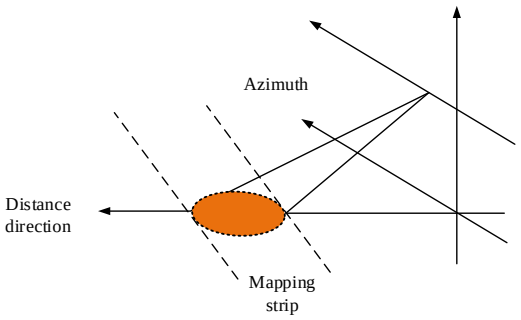

Fig. 1. Schematic diagram of SAR imaging.

In Fig. 1, the azimuth direction is the direction of motion of the SAR carrier platform, while the direction facing the target and perpendicular to the direction of motion is defined as the distance direction. When processing and analyzing SAR images, two important indicators need to be considered first. The first item is the range resolution of SAR, expressed by Formula (1).

$$\rho_r = \frac{D}{2C} \tag{1}$$

In Formula (1), ρ_r represents the distance resolution. D represents the propagation speed of electromagnetic waves. C represents the bandwidth of the transmitted signal. The smaller the C, the higher the distance resolution of the image. The second indicator of SAR images is azimuth resolution, which is expressed by Formula (2).

$$\rho_a = \frac{\lambda S}{2E} \tag{2}$$

In Formula (2), ρ_a represents the azimuth resolution. λ represents the pulse wavelength. S represents the distance between the radar and the target. E represents the antenna aperture. SAR utilizes the motion of the carrier to emit electromagnetic signals at equal intervals and receive echo storage, ultimately performing synthesis processing, thereby achieving high resolution in the azimuth direction. According to the above analysis, SAR essentially utilizes processed surface targets to reflect electromagnetic wave signals to obtain information. Different objects exhibit their unique backward scattering properties when exposed to radar waves due to their unique shapes and materials. These attributes are

displayed at different intensity levels in SAR images, thereby utilizing the grayscale differences of pixels within the image to identify various different targets on the surface. However, the images formed by SAR during high-speed motion may exhibit coherent speckle noise in Fig. 2.

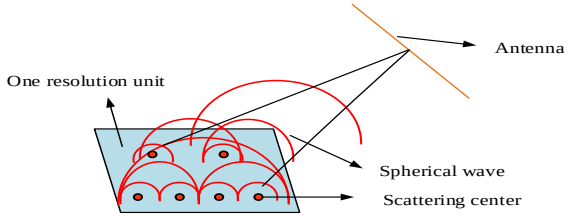

Fig. 2. SAR image coherent speckle noise.

In Fig. 2, the SAR system periodically emits electromagnetic waves. These waves are modulated by the different backscattering properties of the target area through reflection. When the reflected wave returns, the waves generated by various scattering points overlap with each other, causing interference. The interference causes the amplitude of waves to be enhanced in some areas and weakened in others, resulting in wave vectors that exhibit varying degrees of fluctuation in amplitude and phase [14]. SAR images are severely affected by speckle noise, resulting in a significant decrease in image quality. Therefore, this study uses FCM to process SAR images, which helps to preserve the original features of the image and suppress image noise. FCM is obtained by weighting and improving the membership degree of fuzzy clustering, represented by Formula (3) [15].

$$J(U,V)=\sum_{k=1}^{c}\sum_{i=1}^{n}u_{ki}{}^{m}(d_{ki})^{2} \tag{3}$$

In Formula (3), J represents the objective function of FCM. U represents a hard partition matrix. u_{ki} represents the probability of pixels in the cluster center. V represents the set of cluster center vectors. d_{ki} represents the degree of difference between elements and cluster centers. In image processing, the image size is $M*N$, and the total pixels are n. FCM uses the weighted sum of grayscale differences from all pixels to each cluster center to construct the objective function, represented by Formula (4).

$$\begin{cases} J_{FCM}(U,V)=\sum_{k=1}^{c}\sum_{i=1}^{n}u_{ki}{}^{m}\left\|x_i-v_k\right\|^{2} \\ u_{ki}=\sum_{l=1}^{c}\left((x_i-v_k)/(x_i-v_l)\right)^{-2/(m-1)} \\ v_k=\sum_{i=1}^{n}u_{ki}{}^{m}x_i/\sum_{i=1}^{n}u_{ki}{}^{m} \end{cases} \tag{4}$$

In Formula (4), $J_{FCM}(U,V)$ represents the compactness of image clustering. m represents the fuzzy index, which generally takes a value of 2. $\left\|x_i-v_k\right\|^{2}$ represents the Euclidean distance between pixels and cluster centers. x_1 represents image pixels. v represents the cluster center. FCM can achieve fast clustering in image processing, with advantages such as simplicity and convenience. But FCM still has certain limitations in dealing with noise interference and parameter settings. Therefore, the study further improves FCM.

B. Fuzzy C-Means Algorithm Based on Texture Layering Improvement

A Fuzzy Local Information C-means for Gabor Textures Algorithm (GT-FLICM) is proposed to enhance the anti-interference performance of FCM in image processing. The study first uses logarithmic operations to process image noise, converting multiplicative noise into additive noise. The logarithmic operation is performed on the image to obtain the logarithmic difference graph, represented by Formula (5).

$$I_{LR}=\left|\log(I_2(M,N)+1)-\log(I_1(M,N)+1)\right| \tag{5}$$

In Formula (5), I represents SAR image. I_{LR} represents image differences. The Gabor filter and I_{LR} are convolved. To reduce redundancy, the response with the highest amplitude is selected in all directions. Each group of responses is transformed into a column, and the eigenvector matrix Z is obtained. Compared to traditional FCM, GT-FLICM introduces more domain information and uses the grayscale and spatial information of pixels and adjacent pixels for clustering. The definition is represented by Formula (6).

$$J_m=\sum_{i=1}^{n}\sum_{j=1}^{c}(u_{ji}^{m}d^{2}(x_i,v_j)+G_{ki}) \tag{6}$$

In Formula (6), G_{ki} represents the fuzzy factor containing spatial information, represented by Formula (7).

$$G_{ki}=\sum_{j\in n}(1-u_{kj})^{m}\left\|x_j-v_k\right\|^{2}/(d_{ij}+1) \tag{7}$$

The membership matrix for iterative updates and the update formula for cluster centres are calculated using the Lagrange multiplier method, represented by Formula (8).

$$\begin{cases} u_{ki}=1/\sum_{j=1}^{c}\left((\left\|x_i-v_k\right\|^{2}+G_{ki})/(\left\|x_i-v_j\right\|^{2}+G_{ji})\right)^{1/(m-1)} \\ v_k=\sum_{i=1}^{n}u_{ki}{}^{m}x_i/\sum_{i=1}^{n}u_{ki}{}^{m} \end{cases} \tag{8}$$

Through the construction of the aforementioned GT-FLICM, the introduction of blur factors can automatically set weights based on regional characteristics and achieve a good balance between image details and noise, resulting in a good segmentation effect. For the constructed GT-FLICM, when performing change detection on images, the algorithm is evaluated using three indicators: SA, Partition Coefficient (V_{pc}), and Partition Entropy (V_{pe}) [16]. SA represents the ratio of the sum of pixels classified into the correct category in the segmented image to the image's total pixels, expressed by

Formula (9).

$$SA = \sum_{i=1}^{c} (A_i \cap B_i) / \sum_{j=1}^{c} B_j \tag{9}$$

In Formula (9), c represents categories number in which the image is segmented, i.e. the cluster centers number. A_i represents pixels number assigned to class i. B_i represents pixels number of the reference images that belong to class i. V_{pc} and V_{pe} are represented by Formula (10).

$$\begin{cases} V_{pc} = \sum_{k=1}^{c} \sum_{i=1}^{n} u_{ki}^{\ 2} / n \\ V_{pc} = -\sum_{k=1}^{c} \sum_{i=1}^{n} (u_{ki} \lg u_{ki}) / n \end{cases} \tag{10}$$

According to Formulas (9) and (10), the higher the SA, the greater the proportion of pixels correctly classified into their respective categories in the total pixels, and the better the segmentation effect. The larger the V_{pc} and the smaller the V_{pe}, the higher the compactness of the divided internal data, while there are significant differences between different categories, indicating better clustering performance. Fig. 3 shows the ICD method constructed above.

In Fig. 3, the original SAR image is first pre-classified using logarithmic difference maps and GT-FLICM. Then, the classification samples are trained using a neural network. Finally, the ICD results are completed. In sample training, the construction of neural networks will directly affect the result graph's quality. Therefore, the study analyzes and optimizes neural networks.

C. Analysis of Image Change Detection Based on Improved WCNN

The common method in sample training of neural networks is CNN. However, a traditional CNN is difficult to preserve the texture information of the image, and the ability to handle noise is relatively poor [17]. WCNN is adopted. to further improve network performance. A CA module is introduced to extract image features more effectively, and MSCA-WCNN is proposed in Fig. 4.

In Fig. 4, first, the sample is convolved using convolution kernels with different dilation rates to obtain features of different scales of the sample. Under the same convolution kernel, dilated convolution has a larger receptive field compared to regular convolution, which can input more feature information in a single convolution process. The neural network uses a set of 3*3 convolutional kernels with expansion rates of 1, 2, and 5 for operation. Fig. 5 shows the dilated convolution structure.

Fig. 5 (a) shows the receptive field range of dilated convolution and ordinary convolution. The receptive field of regular convolution is 3*3, while the receptive field range of dilated convolution is 5*5, which can process more information. Fig. 5 (b) shows convolutions with different dilation rates. All three sets of dilation convolutions meet the HDC design structure, preserving all pixels of the target while considering the size of the target. The study re-weights the convolution results of each scale through the CA module and then fuses the convolution results based on pixels in Fig. 6.

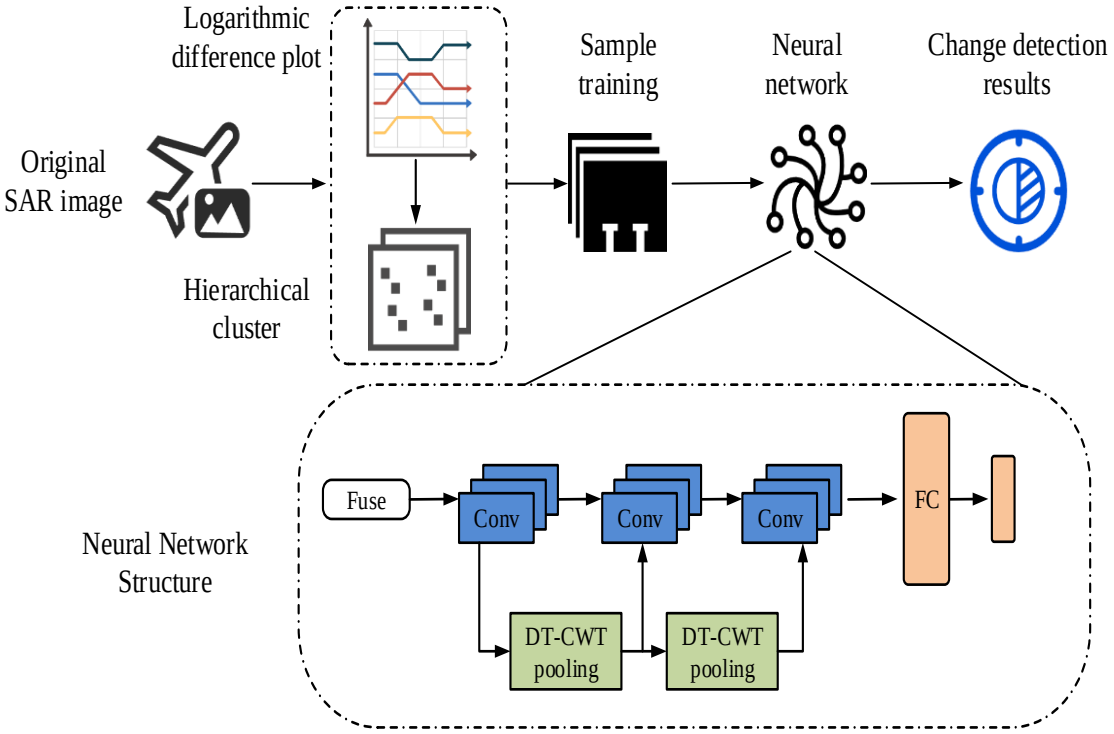

Fig. 3. Framework of image change detection method.

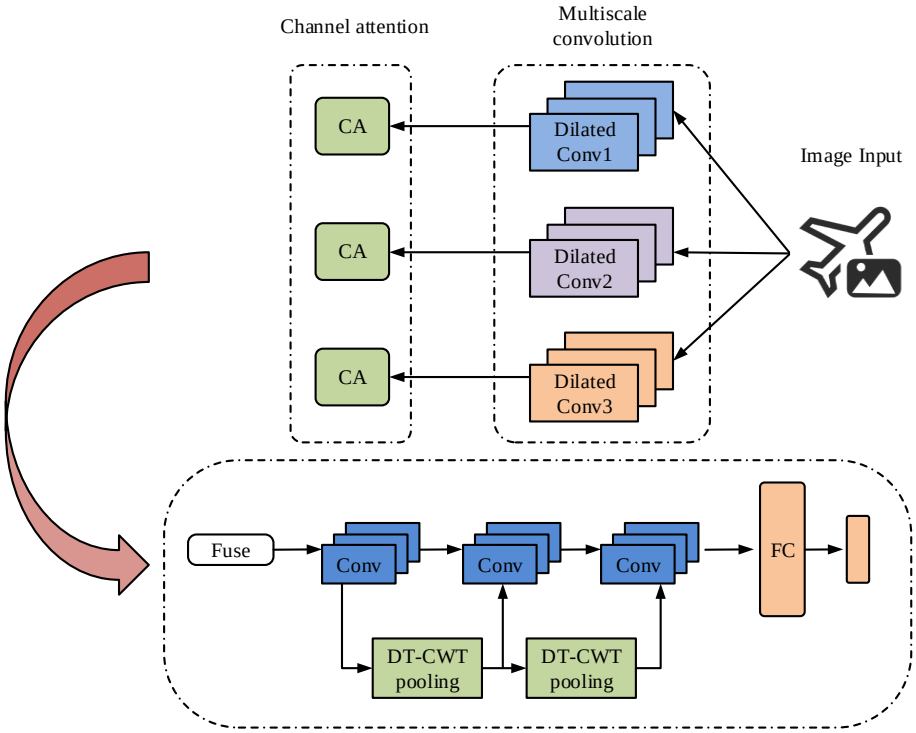

Fig. 4. Schematic diagram of MSCA-WCNN.

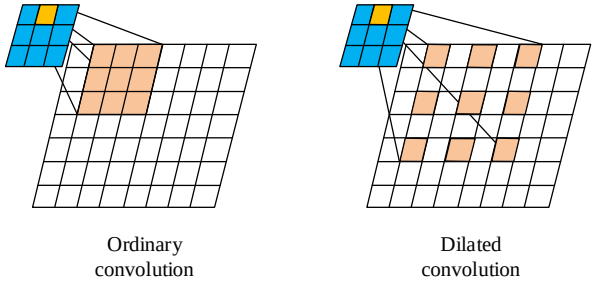

(a) The receptive field range of dilated convolution and ordinary convolution

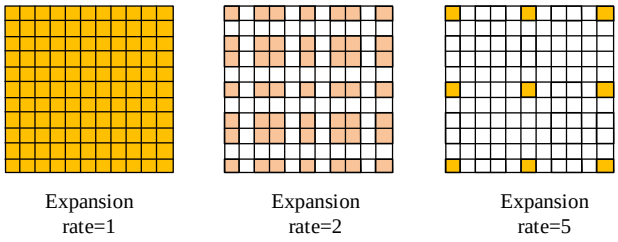

(b) Convolutions with different expansion rates

Fig. 5. Schematic diagram of dilated convolution.

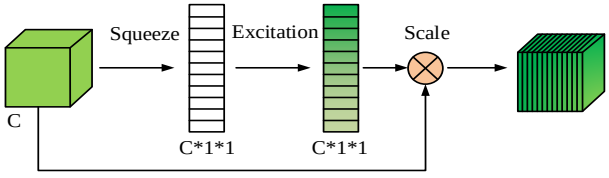

Fig. 6. CA module structure.

In Fig. 6, the CA module displays three key steps, namely squeezing, excitation, and re-weighting. Firstly, the CA module utilizes a global pooling layer to squeeze the input features. The output values obtained are then excited using one-dimensional convolution and Sigmoid functions to analyze the relationships between channels and obtain channel weighted vectors. The feature vector after channel weighting is represented by Formula (11).

$$F_{out} = V \otimes F_{GAP} \quad (11)$$

In Formula (11), V represents the channel weighted vector. F_{GAP} is the output value after the extrusion operation. The expression for multi-scale feature fusion is obtained by summing different channels at the pixel level, represented by Formula (12).

$$F = F_{out}^{1} + F_{out}^{2} + F_{out}^{3} \quad (12)$$

Through the processing of the ASR image mentioned above, the input image is first pre-classified. The processed image is introduced into the neural network structure for feature extraction and sample training. Then, the structure with the feature map is retained. The structure with a large amount of noise is discarded. Finally, the change detection of the image is completed.

IV. Performance Analysis of Image Change Detection Model Based on GT-FLICM and MSCA-WCNN

Firstly, the model was trained and tested using the SAR image dataset. SA, V_{pc}, and V_{pe} were used as performance evaluation metrics to demonstrate the model feasibility. Secondly, five algorithms were used as comparative algorithms to verify the model segmentation performance. Finally, the model was analyzed for practical application.

A. Analysis of Training Results Based on Image Change Detection Models

This study selected the Ottawa dataset for model training and testing to analyze the proposed ICD model. In Ottawa, SAR images had the characteristics of a large number of detail regions, significant noise differences, and small change regions, which verified the algorithm's ability to extract features, resist noise, and maintain stability. Five comparative algorithms included FCM, Fuzzy Local Information C-means (FLICM), Principal Component Analysis Clustering (PCAK), Gabor Principal Component Analysis Network (GaborPCANet), and Enhanced Fuzzy C-means (EnFCM) [18-20]. The algorithm parameters were be unified to ensure the fairness of algorithm comparison experiments. The fuzzy index was 2, the maximum iteration of clustering was 100, the iteration stop threshold was $10e^{-5}$, the penalty weight was 2, and the domain window size was 3*3. Fig. 7 shows the image segmentation performance of different algorithms in the Ottawa dataset.

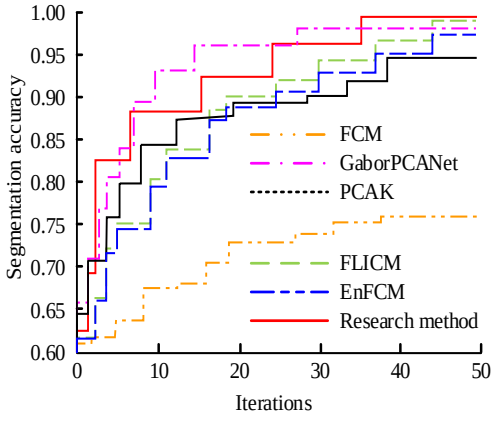

(a) Different algorithm segmentation accuracy results

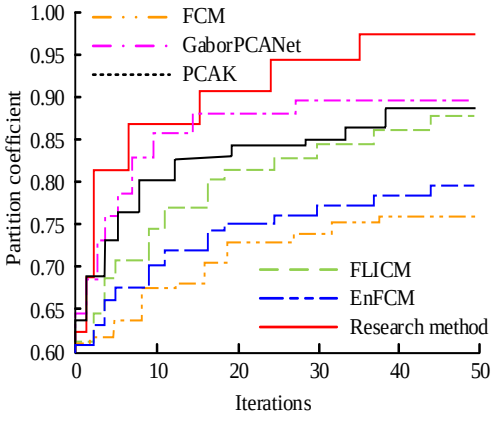

(b) Different algorithm partition coefficient results

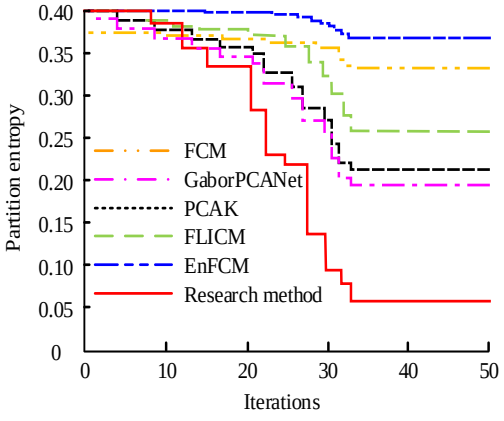

(c) Different algorithm partition coefficient results

Fig. 7. Image segmentation performance of different algorithms.

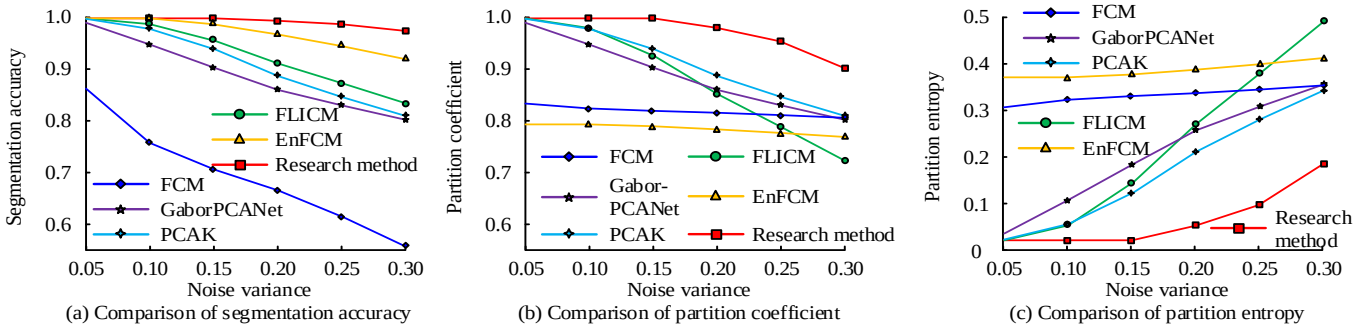

(a) Comparison of segmentation accuracy (b) Comparison of partition coefficient (c) Comparison of partition entropy

Fig. 8. Performance of different algorithms in noisy images.

Fig. 7 (a) shows the SA of different algorithms. The SA of traditional FCM was the lowest, while the SA of other algorithms was not less than 0.900. GT-FLICM had the highest SA of 0.995. Fig. 7 (b) shows the V_{pc} of different algorithms. The V_{pc} of EnFCM was 0.796, which was 0.179 lower than that of GT-FLICM. Fig. 7 (c) shows the V_{pe} of different algorithms. The V_{pe} of GT-FLICM was 0.059. Among the comparative algorithms, only the proposed algorithm had a V_{pe} less than 0.1. Therefore, GT-FLICM had good performance in SARICD tasks, effectively processing detailed regions and extracting accurate change information. A study was conducted to validate the model by incorporating multiplicative noise with different variances to demonstrate the algorithm's processing performance in images with different levels of noise. The variance range of noise was within [0.05, 0.30]. Fig. 8 shows different algorithms' performance.

Fig. 8 (a) shows the SA of the algorithms under different noise variance conditions. When the noise variance was 0.05, the SA of FCM was 0.876, and other algorithms were not less than 0.90. The SA of GT-FLICM was 0.995. When the noise variance was 0.30, the SA of FCM decreased to 0.553, while the SA of PCAK, GaborPCANet, and EnFCM were all below 0.900. The SA of GT-FLICM and FLICM were 0.982 and 0.914, respectively. Fig. 8 (b) shows the V_{pc} of each method under different noise variance conditions. When the noise variance was 0.05, the V_{pc} of EnFCM was 0.793. When the noise variance was 0.30, the V_{pc} of FLICM was 0.725, and the V_{pc} of GT-FLICM was 0.908. Fig. 8 (c) shows the V_{pe} of the algorithms under different noise variances. When the noise variance was 0.05, the V_{pe} of EnFCM was 0.384, which was 0.347 higher than that of GT-FLICM. When the noise variance was 0.30, the V_{pe} of GT-FLICM was 0.192, and the V_{pe} of other comparison algorithms was not less than 0.300. Therefore, GT-FLICM had relatively stable and excellent processing performance in images with varying noise, maintaining high SA and low V_{pe}, which was a more reliable method in SARICD. The study analyzed the algorithmic iteration in Fig. 9.

In Fig. 9, as the noise variance increased, the iterations of each algorithm also increased. FCM increased from 44 to 62 times. FLICM increased from 33 to 70 times. PCAK increased from 24 to 40 iterations. GaborPCANet increased from 28 to 61 iterations. EnFCM increased from 22 to 84 times. GT-FLICM increased from 18 to 36 times. Therefore, GT-FLICM had faster computational efficiency and certain anti-interference ability in the face of noise.

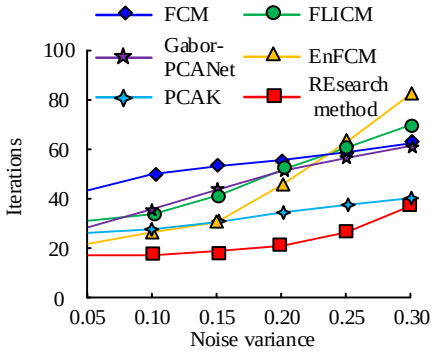

Fig. 9. Iteration speed of different algorithms

B. *Application Effect Analysis Based on Image Change Detection Model*

The ICD model based on GT-FLICM and MSCA-WCNN achieved good results in the training set. Real SAR images were used to analyze the model to verify the feasibility of the model's practical application. The real images, river and farmland images, were analyzed. Fig. 10 shows the detection effect on river images.

Fig. 10 (a) shows the original river image and the river images processed by various algorithms. FCM had the worst segmentation performance, with a large number of misclassified pixels on both sides of the image. FLICM, PCAK, GaborPCANet, and EnFCM improved noise resistance to varying degrees. The images of FLICM, PCAK, GaborPCANet, and EnFCM had fewer misclassified pixels on both sides, but these methods still struggled to meet practical application needs. The proposed method utilized local information to adaptively suppress noise, resulting in fewer misclassified pixels in the image and better regional completion. Fig. 10 (b) shows the segmentation performance of various algorithms in river images. The results of Fig. 10 (b) were consistent with those in Fig. 10 (a), and the proposed algorithm had the best segmentation performance, with SA of 0.983, V_{pc} of 0.935, and V_{pe} of 0.135. Fig. 11 shows the change detection effect on farmland images.

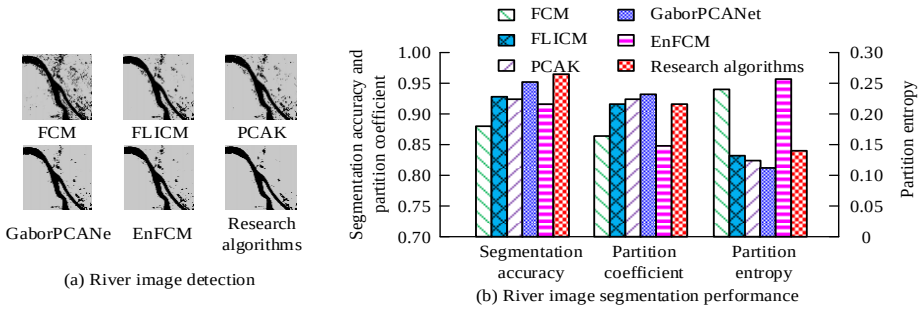

Fig. 10. Change detection effect of river images.

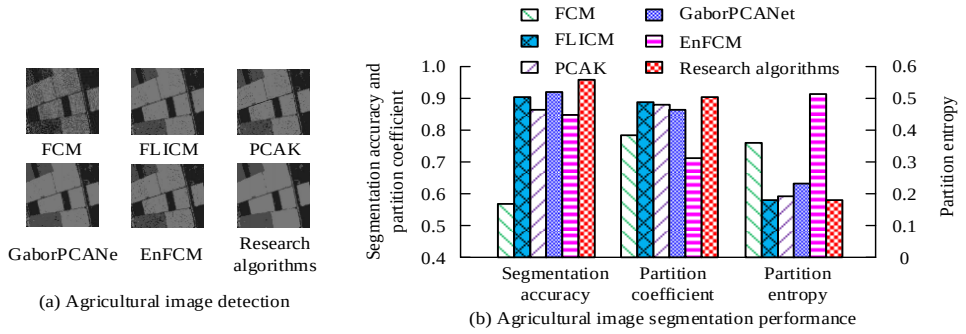

Fig. 11. Change detection effect of farmland images

Fig. 11 (a) shows the original farmland image and the farmland images processed by various algorithms. FCM was most affected by speckle noise and had the worst visual effect. FLICM, PCAK, GaborPCANet, and EnFCM all had misclassified pixels in each region of the image due to the presence of speckle noise. Especially in the light gray and dark gray areas, the misclassified pixels seriously affected the region integrity. The proposed method achieved the best visual effect between noise suppression and preserving image details, with only few pixels being misclassified in each category. Fig. 11 (b) shows the segmentation performance of various algorithms in farmland images. The results of Fig. 11 (b) and 11 (a) were consistent, and the proposed algorithm had the best segmentation performance, with SA of 0.960, V_{pc} of 0.902, and V_{pe} of 0.183. Based on the detection results of river and farmland images, the advantages of GT-FLICM and MSCA-WCNN in real SAR images were reflected in their good noise resistance, improved regional integrity of images, and high segmentation performance. Finally, the study conducted ablation experiments on the model by calculating complexity and running time efficiency in Table I.

TABLE I. CALCULATION COMPLEXITY AND RUNTIME EFFICIENCY

Algorithm	Time complexity	Space complexity	Operating efficiency
FLICM	O(cbMNr)	O(cbMNr)	0.53s
Hierarchical FLICM method	O((c1b1+c2b2) MNr)	O((c1b1+c2b2) MNr)	0.71s
GT-FLICM	O((c1b1r+c2b2r+MNsk) MN)	O((c1b1r+c2b2r+MNsk) MN)	0.88s

In Table I, c refers to the categories number. M and N represent the image size. R refers to the local window size. B represents iteration. In FFLICM, the time and spatial complexity were both O(cbMNr). Compared to traditional FLICM, the layered FLICM method added one more classification process, resulting in a time and spatial complexity of O((c1b1+c2b2)MNr). In GT-FLICM, the complexity of the Gabor texture process was O(skMNHW). s refers to the size, k refers to the direction, and HW refers to the size of the Gabor kernel. Therefore, the time and spatial complexity of GT-FLICM was O ((c1b1r+c2b2r+MNsk) MN). Although the time complexity of GT-FLICM increased to some extent, the time only increased by 0.35s in image processing speed. Combined with comprehensive detection performance, GT-FLICM exhibited good performance.

V. DISCUSSION

According to the above experimental results, the study is improved by introducing fuzzy membership degree and Gabor texture feature. GT-FLICM performed well in high noise environment. The traditional method has limited effect on speck noise suppression. GT-FLICM combines wavelet transform and multi-scale attention mechanism to improve SA while preserving image details. GT-FLICM has the most obvious advantage in the iterations. When the noise variance was 0.30, GT-FLICM only needed 36 iterations, while other methods had more than 40 iterations. The results show that GT-FLICM has significant advantages in computing efficiency. In river image detection, the performance of traditional algorithms such as FCM was poor in noisy environment, and there were too many misclassified pixels. GT-FLICM used

local information adaptive suppression of noise, less misclassified pixels, and improved regional integrity. Therefore, compared with traditional methods, combining fuzzy membership degree, Gabor texture features, and multi-scale CA mechanism can effectively solve the SAR ICD under high noise environment. The high SA and low classification error rate provide reliable support for practical applications. Although GT-FLICM performs well in computational efficiency, with the increase of dataset size, the computational complexity may become a bottleneck. Future research can further optimize the algorithm by introducing parallel computing, model compression, and other technical means to improve the efficiency of processing large-scale datasets. The excellent performance of the model in river and farmland images shows the potential of the model in practical applications such as environmental monitoring and geological exploration.

VI. CONCLUSION

This study proposed an ICD model combined improved FCM with MSCA-WCNN for the coherent speckle noise in SARICD. The model introduced fuzzy membership degree and Gobor texture to improve FCM, while introducing multi-scale CA mechanism to improve WCNN. GT-FLICM achieved 0.995 SA, 0.975 V_{pc}, and 0.059 V_{pe} on Ottawa. When the noise variance was 0.30, the three segmentation indicators of GT-FLICM were 0.995, 0.975, and 0.192, respectively. In the iterative experiment, GT-FLICM only needed 36 iterations, which showed a significant improvement compared to other comparative algorithms. In practical applications, the detection results of GT-FLICM in river and farmland images demonstrated the efficient noise resistance and excellent segmentation performance, and the algorithmic running time was only 0.88 seconds. The results show that the improved FCM algorithm can effectively improve the suppression ability of speckle noise by combining fuzzy membership degree and Gabor texture feature. The multi-scale CA mechanism enhances the model's focus on important features by weighting features. The multi-scale CA mechanism not only improves the detection accuracy and stability of the model under different noise levels, but also can better process the multi-scale information in the image to ensure the detection effect in the complex environment. However, there are still shortcomings in the research. The algorithm combines multiple methods and has high computational complexity. When facing large-scale datasets, the time efficiency still needs to be improved. Future research directions should focus on optimizing algorithm computational efficiency and reducing algorithm runtime.

REFERENCES

[1] Löw F, Dimov D, Kenjabaev S, Zaitov S, Stulina G, Dukhovny V. Land cover change detection in the Aralkum with multi-source satellite datasets. GIScience & Remote Sensing, 2022, 59(1): 17-35.

[2] Connetable P, Conradsen K, Nielsen A A, Skriver H. Test statistics for reflection symmetry: Applications to quad-polarimetric SAR data for detection of man-made structures. IEEE Journal of Selected Topics in Applied Earth Observations and Remote Sensing, 2022, 15(4): 2877-2890.

[3] Karaman K, Sainte Fare Garnot V, Wegner J D. Deforestation detection in the Amazon with sentinel-1 SAR image time series. ISPRS Annals of the Photogrammetry, Remote Sensing and Spatial Information Sciences, 2023, 10(1): 835-842.

[4] Chen T, Lu Z, Yang Y, Zhang Y, Du B, Plaza A. A Siamese network based U-Net for change detection in high resolution remote sensing images. IEEE Journal of Selected Topics in Applied Earth Observations and Remote Sensing, 2022, 15(2): 2357-2369.

[5] Ghosh C, Majumdar D, Mondal B. A deep learning-based SAR image change detection using spatial intuitionistic fuzzy C-means clustering. Transactions in GIS: TG, 2022. 26(6):2519-2535.

[6] Su H, Zhang X, Luo Y, Zhang C, Zhou X, Atkinson P. Nonlocal feature learning based on a variational graph auto-encoder network for small area change detection using SAR imagery. ISPRS journal of photogrammetry and remote sensing, 2022, 193(5):137-149.

[7] Li W T, Pang B, Xu X, Wei B. A SAR change detection method based on an iterative guided filter and the log mean ratio. Remote sensing letters, 2022, 13(7/9):663-671.

[8] Wang J, Gao F, Dong J, Zhang S, Du Q. Change detection from synthetic aperture radar images via graph-based knowledge supplement network. IEEE Journal of Selected Topics in Applied Earth Observations and Remote Sensing, 2022, 15(4):1823-1836.

[9] Ghosh C, Majumdar D, Mondal B. Detection of changes in synthetic aperture radar images using Modified Gauss-Log ratio and Fuzzy Local Information C-Means clustering. Multimedia Tools and Applications, 2023, 82(27): 42661-42678.

[10] Peng Y, Cui B, Yin H, Zhang Y, Du P. Automatic SAR change detection based on visual saliency and multi-hierarchical fuzzy clustering. IEEE Journal of Selected Topics in Applied Earth Observations and Remote Sensing, 2022, 15(4): 7755-7769.

[11] Yi W, Wang S, Ji N, Wang C, Xiao Y, Song X. SAR image change detection based on Gabor wavelets and convolutional wavelet neural networks. Multimedia Tools and Applications, 2023, 82(20): 30895-30908.

[12] Zhang W, Jiao L, Liu F, et al. Adaptive contourlet fusion clustering for SAR image change detection. IEEE Transactions on Image Processing, 2022, 31(2): 2295-2308.

[13] Peng Y, Wei Z, Cui B. Unsupervised SAR Change Detection Method Based on Refined Sample Selection. ISPRS Annals of the Photogrammetry, Remote Sensing and Spatial Information Sciences, 2022, 3(1): 665-672.

[14] Zhou Y, Yang K, Ma F, Hu W, Zhang F. Water–land segmentation via structure-aware CNN–transformer network on large-scale SAR data. IEEE Sensors Journal, 2022, 23(2): 1408-1422.

[15] Selvam N, Nagesa Y, Negesa F. Deep learning approach with optimization algorithm for reducing the training and testing time in SAR image detection and recognition. Indian J. Sci. Technol, 2022, 15(9): 371-385.

[16] Wu Y, Xu Q, Zhang Z, Ma J, Zhao T, Zhu X. SAR Change Detection Algorithm Combined with FFDNet Spatial Denoising. Journal of Environmental & Earth Sciences, 2023, 5(2): 88-101.

[17] Choudhuri S, Adeniye S, Sen A. Distribution Alignment Using Complement Entropy Objective and Adaptive Consensus-Based Label Refinement For Partial Domain Adaptation. Artificial Intelligence and Applications. 2023, 1(1): 43-51.

[18] Song Q, Wu C, Tian X, Song Y, Guo X. A novel self-learning weighted fuzzy local information clustering algorithm integrating local and non-local spatial information for noise image segmentation. Applied Intelligence, 2022, 52(6): 6376-6397.

[19] Aliradi R, Ouamane A. A novel descriptor (LGBQ) based on Gabor filters. Multimedia Tools and Applications, 2024, 83(4): 11669-11686.

[20] Zhang C, Chen L, Zhao Y P, Wang Y, Chen C L P. Graph enhanced fuzzy clustering for categorical data using a Bayesian dissimilarity measure. IEEE Transactions on Fuzzy Systems, 2022, 31(3): 810-824.